Novel Third-Order Distortion Generator with Residual IM2 Suppression Capabilities

Wei Huang, *Member, IEEE,* and Ricardo E. Saad, *Member, IEEE*

***Abstract*— Commonly used diode-based third-order distortion generators produce residual second-order distortion signals due to the unmatched statistical characteristics of the diodes. In this paper, a novel circuit technique is presented by which, in theory, the suppression of undesirable residual second-order distortion is achieved. A theoretical analysis of the proposed novel circuit topologies is carried out using Volterra series analysis. The residual second-order intermodulation distortions (IM2) of conventional antiparallel and bridge configurations are compared with the modified versions presented in the paper. Simulated results show that the modified antiparallel configuration possess a maximum residual IM2 46 dB lower than the one produced by the conventional configuration. The modified bridge configuration has a maximum residual IM2 36 dB lower than the one of the conventional configuration. A sensitivity analysis of the modified configurations is also presented. Experimental results indicate that 20-dB cancellation is achievable.**

***Index Terms*— Intermodulation, linearization, predistortion, second-order cancellation, third-order distortion generator, Volterra analysis.**

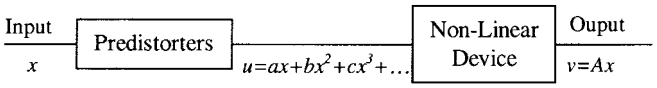

Fig. 1. Block diagram illustrating the predistotion technique.

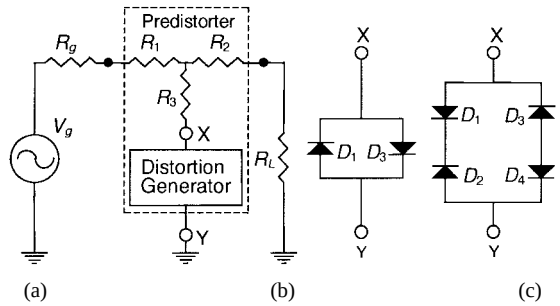

Fig. 2. (a) Third-order predistorter configuration, (b) conventional antiparallel generator, and (c) conventional bridge generator. DC bias circuits are not shown.

I. Introduction

SIGNAL predistortion is a widely used linearization technique which has found application in the design of highly linear analog optical transmitters such as the ones used in CATV [1]–[3], and microwave links [4] as well as in the design of high power amplifiers utilized in wireless communications and microwave radio systems [5]. The technique consists of inserting a set of predistorters before the device to be linearized, as shown in Fig. 1, such that each predistorter generates a nonlinearity of fixed order whose amplitudes and phases in a frequency range are, respectively, equal and 180° out of phase to the ones produced by the device to be linearized. As a result, the output signal, ideally, is linear (at least, the output signal does not contain the nonlinearity orders of the predistorter). However, in practice, predistorters not only generate the order of the nonlinearity for which they were designed but also generate residual nonlinearities of different orders. These residual nonlinearities may interact with the main nonlinearity introduced by another predistorter (in the case that multiple predistorters are used) or add extra nonlinearities to the overall circuit, which may have a detrimental effect on the performance of the circuit [1]. For that reason, it is important to design predistorters that reduce, as much as possible, the generation of unwanted nonlinearities. In this paper, a novel technique is presented by which the residual second-order intermodulation distortion (IM2) of diode-based third-order generators is substantially reduced. Fig. 2(a) shows a general implementation of a third-order predistorter (TOP). It consists of a third-order-distortion generator and a pad (implemented by resistors R_1, R_2, and R_3) which is utilized to sample the RF signal from the main path and also to inject the nonlinear signal generated by the distortion generator. V_g is the RF voltage source, R_g is the internal resistance of the generator, and R_L is the load. Several types of diode-configurations can be utilized to implement the distortion generator. Fig. 2(b) and (c) shows, respectively, a conventional antiparallel and a conventional bridge configuration [1], [5], [6].

The topologies of the circuits are such that when all the diodes are identical, only third-order distortion is injected to the main path. However, in general, when the diodes are not identical, second-order nonlinearities are generated.[1] The main cause for the unmatched statistical characteristics among diodes of the same type is the dissimilarity of their ideality factors, η. Fig. 3 shows the residual IM2 delivered to the load R_L by a conventional antiparallel predistorter configuration utilizing Schottky diodes as a function of the ideality factor

Manuscript received March 27, 1998; revised August 26, 1998. This work was developed at Harmonic Lightwaves, Inc., Sunnyvale, CA.

W. Huang is with Harmonic Lightwaves, Inc., Sunnyvale, CA 94089 USA.

R. E. Saad was with Harmonic Lightwaves, Inc., Sunnyvale, CA 94089 USA. He is now with Alcatel Network Systems, Richardson, TX 75081 USA.

Publisher Item Identifier S 0018-9480(98)09195-9.

[1] In the bridge configuration, there are two particular cases where even though the diodes are different, there is no residual IM2. This occurs when a) diodes D_1 and D_2, and D_3 and D_4 are, respectively, identical and b) diodes D_1 and D_3, and D_2 and D_4 are, respectively, identical.

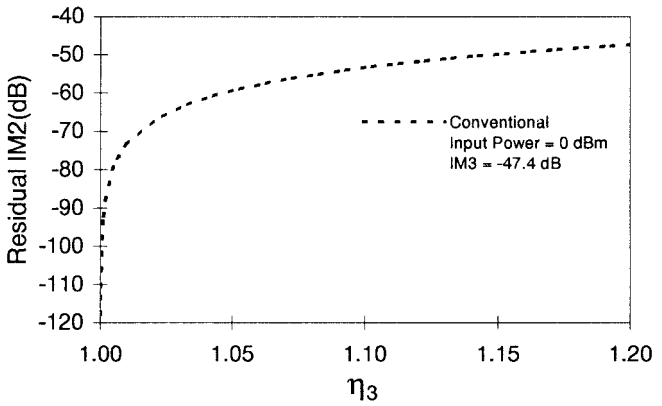

Fig. 3. Residual IM2 as a function of η_3 for the conventional antiparallel configuration.

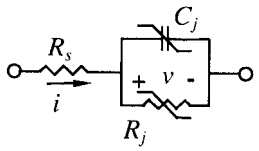

Fig. 4. Equivalent circuit for a Schottky diode.

of diode D_3 (η_3). The simulated results shown in the figure were obtained utilizing the software CNL/2 [7] where it was assumed that the ideality factor of diode D_1 (η_1) is equal to one and η_3 may vary from 1 to 1.2. For the example, it is assumed that the type of diodes utilized to implement the conventional antiparallel configuration have ideality factors whose statistical distribution is in the interval $[\eta_{\min}\ \eta_{\max}]$, where $\eta_{\min}$ and $\eta_{\max}$ are, respectively, the minimum and maximum possible ideality factors for that type of diode. For the example, it is assumed that $\eta_{\min} = 1$ and $\eta_{\max} = 1.2$.

Fig. 4 shows the Schottky diode model utilized in the simulation [8], [9]. R_s, R_j, and C_j are, respectively, the series resistance, and the small signal junction resistance and capacitance. The special symbol utilized over the resistance R_j and capacitance C_j indicates that both elements are nonlinear. For the purposes of the analysis presented in this paper, the effect of C_j is neglected.[2] It should be noted that the frequency range for which the analysis presented here is valid depends on the type of Schottky diodes utilized in the implementation of the circuits. For example, predistorters utilized in CATV applications operate between 5 MHz and 1 GHz. These predistorters, in general, utilize Schottky diodes whose cutoff frequencies are in the tens of gigahertzs. Therefore, for this application (and many others), the effect of the C_j can be neglected. Table I shows the diodes' parameters, the resistor values of the pad, and the currents and voltages utilized in the simulation. I_{B1} and I_{B3} are the dc bias currents of the diodes D_1 and D_3. The subindex utilized for each of the diode parameters indicates with which diode the parameter is associated.

From Fig. 3, it can be noted that the residual IM2 is significantly reduced for values of η_3 smaller than 1.01, and it is completely suppressed when $\eta_3 = 1$. However, for larger values of η_3, the residual IM2 becomes significant. It is important to realize that the residual IM2 of a circuit depends directly on the ideality factors of the diodes that compose the predistorter. Since the ideality factor of diodes of the same type is a random variable, the maximum residual IM2 (MRIM2) for the example shown in Fig. 3 occurs when $\eta_3 = 1.2$ (note that $\eta_1 = 1$). For this case MRIM2 $= -47.4$ dB. Similar results to those shown in Fig. 3 can also be obtained for the bridge configuration.

One approach to reduce the residual IM2 in the circuits previously described consists of adjusting the bias current in some of the diodes such that the measured residual IM2 be reduced to an acceptable level [1]. Another approach is to measure, in a large set of diodes, the ideality factor of each diode and match those with similar ideality factors. Even though these techniques reduce the residual IM2 of the circuits, they are not suitable for high-volume production since they are time-consuming and expensive.

In Section II, novel circuit topologies are presented that substantially reduce the generation of residual IM2. In Section III, a nonlinear analysis of the new topologies is presented based on Volterra series analysis. In Section IV, a sensitivity analysis shows the effects of temperature and bias current variations and component tolerances in the performance of the circuits. Experimental results are shown in Section V.

II. Novel Circuit Topologies

Fig. 5(a) and (b) shows, respectively, two novel circuit topologies that reduce the generation of residual IM2 for the antiparallel and bridge configurations. The modification to the bridge configuration consists of adding a resistor R between the middle nodes of the two branches. The modification to the antiparallel configuration consists of adding two resistors (R_d), in addition to the resistor R, to form a bridge configuration. Qualitatively, the mechanism by which the residual IM2 is reduced in the new topologies can be clearly explained for the case of the modified antiparallel configuration. The objective of the resistive network, implemented by resistor R and two resistors R_d, is to suppress the residual IM2 not only when $\eta_1 = \eta_3 = 1$, as it happens in the conventional configuration (see Fig. 3), but also when $\eta_1 = 1$ and $\eta_3 = C$, where C is a value larger than one (for the example presented in Fig. 3, the constant C should be larger than one and smaller than 1.2). Consequently, the residual IM2 as a function of η_3 will be different from the one shown in Fig. 3. The resistor R in the modified bridge configuration plays a similar role to the resistive network in the modified antiparallel configuration. In the following section, an analytical explanation is presented.

III. Nonlinear Analysis

The analysis of the circuits shown in Fig. 5 is carried out using the method of nonlinear currents based on Volterra series analysis [8]. The method is applicable to the circuits analyzed in this paper because they possess weak nonlinearities. The modified bridge configuration in Fig. 5(b) is analyzed first since, as it will be shown later, the modified antiparallel configuration is a particular case of it.

[2] It is assumed that the circuits are memoryless.

TABLE I
DIODE PARAMETERS, RESISTOR VALUES, CURRENTS, AND VOLTAGES USED IN THE SIMULATION OF THE MODIFIED AND CONVENTIONAL ANTIPARALLEL CONFIGURATIONS

η_{min}	η_{max}	η_1	η_3	R_{S1}	R_{S3}	T
1	1.2	1	1-1.2	5 Ω	5 Ω	300 K
I_{B1}	I_{B3}	$R_1 = R_2$	R_3	R_g	R_L	$P_g = V_g^2/R_g$
1 mA	1 mA	10 Ω	80 Ω	75 Ω	75 Ω	0 dBm

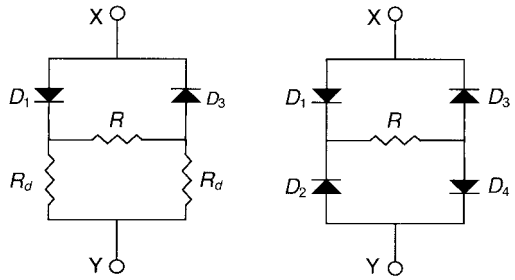

Fig. 5. Proposed new configurations to reduce the MRIM2: (a) modified antiparallel configuration and (b) modified bridge configuration. DC bias circuits are not shown.

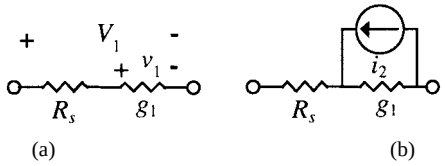

Fig. 6. (a) Linear equivalent circuit and (b) second-order equivalent circuit used to calculate the linear and second-order components using the method of nonlinear currents.

From Fig. 4, neglecting the effect of the nonlinear capacitance C_j, it can be seen that a Schottky diode can be represented by a linear resistance (R_S) in series with a nonlinear resistance (R_j). R_j has a voltage v across it and current i, its current–voltage relation is given by [8], [9]

$$i = g_1 v + g_2 v^2 + g_3 v^3 + \cdots \tag{1}$$

where $g_1 = I_B\alpha$, $g_2 = \frac{1}{2} I_B \alpha^2$, $g_3 = \frac{1}{6} I_B \alpha^3$, and $\alpha = q/\eta kT$. T, q, and k are the junction temperature, the electron charge, and the Boltzman's constant, respectively.

Fig. 6(a) and (b) shows, respectively, the equivalent circuits of a Schottky diode utilized to calculate the first- and second-order components using the method of nonlinear currents. The voltage v_1 is found through linear analysis, assuming that all sources of nonlinearities are set to zero. The second-order current source, $i_2 = g_2 v_1^2$, which represents all the second-order current components in the nonlinear element, is found from the voltage v_1 calculated previously. The voltage V_1 is the total linear voltage across the resistor R_S and the conductance g_1, as shown in Fig. 6(a).

Fig. 7(a) and (b) shows, respectively, the equivalent circuits for the linear and second-order analysis of the TOP using the modified bridge configuration shown in Fig. 5(b). R_e and V_e are the equivalent Thevenin resistance and voltage,

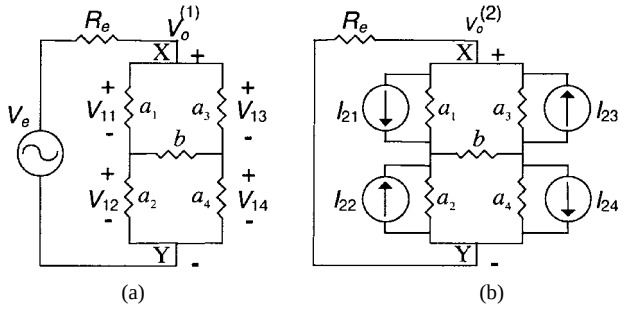

Fig. 7. (a) Linear and (b) second-order equivalent circuits for the bridge configuration using the methods of nonlinear currents.

respectively, between nodes X and Y, $b = 1/R$, and

$$a_k = \frac{g_{1k}}{g_{1k}R_{Sk} + 1} \tag{2}$$

$$V_{1k} = (g_{1k}R_{Sk} + 1)v_{1k} \tag{3}$$

$$I_{2k} = \frac{i_{2k}}{g_{1k}R_{Sk} + 1} = \frac{g_{2k}v_{1k}^2}{g_{1k}R_{Sk} + 1} = \frac{g_{2k}V_{1k}^2}{(g_{1k}R_{Sk} + 1)^3} \tag{4}$$

where the subindex $k = 1, 2, 3, 4$ is associated with the diode numbers as indicated in Fig. 5(b).

From Fig. 7(a), it can be seen that each of the voltages V_{1k} can be expressed as a function of the linear output voltage $V_o^{(1)}$ as follows:

$$V_{11} = \frac{b(a_2 + a_4) + a_2(a_3 + a_4)}{\xi} V_O^{(1)} \tag{5}$$

$$V_{12} = \frac{b(a_1 + a_3) + a_1(a_3 + a_4)}{\xi} V_O^{(1)} \tag{6}$$

$$V_{13} = \frac{b(a_2 + a_4) + a_4(a_1 + a_2)}{\xi} V_O^{(1)} \tag{7}$$

$$V_{14} = \frac{b(a_1 + a_3) + a_3(a_1 + a_2)}{\xi} V_O^{(1)} \tag{8}$$

where

$$\xi = b(a_1 + a_2 + a_3 + a_4) + (a_1 + a_2)(a_3 + a_4). \tag{9}$$

The voltage $V_o^{(1)}$, in turn, can be calculated as a function of V_e as shown in (10) at the bottom of the following page. The voltage $V_o^{(2)}$ indicated in Fig. 7(b) represents the second-order output voltage and it can be found, after a tedious process, as shown in (11) at the bottom of the following page. Note that the voltage $V_o^{(2)}$ can be calculated as a function of the voltage generator by using (4)–(10).

From (11), it can be seen that $V_o^{(2)}$ is reduced to zero when the numerator is equal to zero. A value of $b\ (=1/R)$

can be found that satisfies $V_o^{(2)} = 0$. This indicates that complete cancellation of the second-order distortion can be obtained even though the diodes have different ideality factors. Also, it should be noted that when all diodes are equal ($I_{21} = I_{22} = I_{23} = I_{24}$ and $a_1 = a_2 = a_3 = a_4$), the presence of the conductance b does not affect the cancellation of the second-order distortion.

A. Modified Antiparallel Distortion Generator

For this particular case, the model shown in Fig. 7 can be applied to analyze the modified antiparallel distortion generator shown in Fig. 5(a) by setting $I_{22} = I_{24} = 0$ and $a_2 = a_4 = 1/R_d$. By equating $V_o^{(2)} = 0$, a value of R can be found as shown in (12) at the bottom of this page. R_d should be selected such that $R > 0$. It can be shown that R_d has to be chosen such that (see Appendix A)

$$R_d \geq \frac{g_{11}^{1/3} + g_{13}^{1/3}}{g_{11}^{2/3}\, g_{13}^{2/3}} - R_S = R_{d\,\min} \tag{13}$$

where $R_{d\,\min}$ is the minimum value of R_d. For $R_d = R_{d\,\min}$, $R \rightarrow \infty$. Therefore, the suppression of the residual IM2 ($V_o^{(2)} = 0$) can be achieved without the need of the resistor R. In general, the value of R_d should not be too large since, in that case, the third-order intermodulation (IM3) is substantially reduced in comparison to the IM3 of the conventional configuration under similar bias conditions.

Fig. 8 shows the residual IM2 (at R_L) as a function of η_3 when the TOP [Fig. 2(a)] is utilized in conjunction with the modified antiparallel distortion generator [Fig. 5(a)] and the conventional one [Fig. 2(b)]. For both cases, the parameters shown in Table I were utilized in the simulation. For the modified antiparallel configuration, $R_d = 60\ \Omega$ and $R = 686\ \Omega$. The value of R was calculated using (12) and assuming that $\eta_1 = 1$ and $\eta_3 = 1.2$. It should be noted that for the antiparallel configuration, the residual IM2 is totally suppressed when η_3 is 1 and 1.2. From Fig. 8, it can be observed that the MRIM2 occurs at $\eta_3 = 1.1$. The residual IM2 at that point is -93.5 dB. This value is 46.1 dB smaller than the MRIM2 of the conventional antiparallel configuration (note that in Fig. 3, MRIM2 $= -47.4$ dB). The penalty for adding the resistors R and R_d is a 1.5 dB reduction of the IM3 delivered to the load in comparison to the one delivered by a conventional antiparallel configuration under similar conditions. However, in most cases, this penalty can be easily compensated by biasing the diodes at lower currents or by increasing the input signal power.

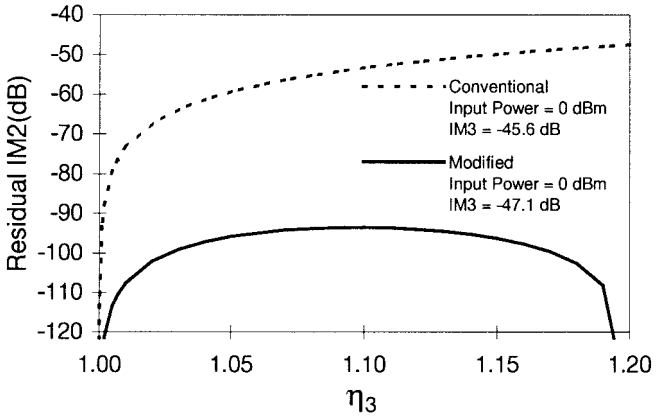

Fig. 8. Simulation results for the (a) conventional and (b) modified antiparallel configuration.

The simulation results shown in Fig. 8 for the modified antiparallel configuration case assume that the resistor R is calculated with $\eta_3 = 1.2$. Fig. 9 shows the cases where R is calculated with $\eta_3 = 1.1$, 1.15, 1.17, and 1.2.[3] As can be observed, if the resistor R is calculated assuming that $\eta_3 = 1.1$ or 1.15 and the maximum (statistical) value of η_3 can be as high as 1.2, the MRIM2 for both cases is larger than the one corresponding to the case where R is calculated with $\eta_3 = 1.2$. However, if R is calculated with $\eta_3 = 1.17$, the MRIM2 is slightly smaller than the one corresponding to the case where the resistor R is calculated with $\eta_3 = 1.2$. From a theoretical point of view, the optimum case occurs when R is calculated with $\eta_3 = 1.17$. However, from a practical point of view, there are other factors, such as temperature variation

[3]It should be noted that even though the calculation of R is carried out at $\eta_3 < 1.2$, it is still assumed that the statistical distribution of η_3 is between 1 and 1.2.

$$V_O^{(1)} = \frac{V_e}{1 + R_e \dfrac{a_1[b(a_1+a_2)+a_2(a_3+a_4)] + a_3[b(a_2+a_4)+a_4(a_1+a_2)]}{\xi}} \tag{10}$$

$$V_O^{(2)} = \frac{-[a_2(b+a_3+a_4)+ba_4]I_{21} + [a_1(b+a_3+a_4)+ba_3]I_{22} + [a_4(b+a_1+a_2)+ba_2]I_{23} - [a_3(b+a_1+a_2)+ba_1]I_{24}}{a_1[a_2(b+a_3+a_4)+ba_4] + a_3[a_4(b+a_1+a_2)+ba_2] + \dfrac{\xi}{R_e}} \tag{11}$$

$$R = \frac{2\left[g_{11}^{2/3}(g_{13}R_s+1) - g_{13}^{2/3}(g_{11}R_s+1)\right]}{g_{13}^{2/3}\left[\dfrac{1}{R_d}(g_{11}R_s+1) + g_{11}\right] - g_{11}^{2/3}\left[\dfrac{1}{R_d}(g_{13}R_s+1) + g_{13}\right]} \tag{12}$$

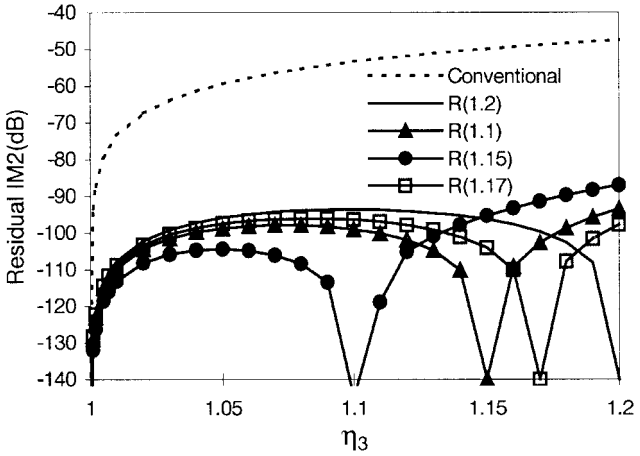

Fig. 9. Residual IM2 as a function of η_3 for the antiparallel configuration for different values of R. The value of η_3 utilized to calculate the resistance is shown in parentheses. The residual IM2 for the conventional configuration is shown for comparison purposes.

and component tolerances, which affect more significantly the overall performance of the circuit, reducing the importance of determining R with $\eta_3 = 1.17$ or 1.2. The effects of those factors in the performance of the circuit are shown in Section IV.

B. Modified Bridge Distortion Generator

Assuming that the statistical distribution of the ideality factors of a particular type of diodes is between $\eta_{\min}$ and $\eta_{\max}$, it can be proven that the MRIM2 of the conventional bridge configuration occurs when the diodes utilized to implement the bridge satisfy the following conditions: $\eta_1 = \eta_4$, $\eta_2 = \eta_3$, $\eta_1 \neq \eta_2$, where $\eta_1 = \eta_{\min}$ and $\eta_2 = \eta_{\max}$ (or alternatively, $\eta_1 = \eta_{\max}$ and $\eta_2 = \eta_{\min}$). For this particular case, $a_1 = a_4$, $a_2 = a_3$, $I_1 = I_4$, and $I_2 = I_3$. By equating $V_o^{(2)} = 0$, a value of R can be found as follows[4]:

$$R = \frac{g_{11}^{2/3}(g_{12}R_s + 1) - g_{12}^{2/3}(g_{11}R_s + 1)}{g_{11}g_{12}^{2/3} - g_{12}g_{11}^{2/3}}. \tag{14}$$

Fig. 10 shows the residual IM2 (at R_L) as a function of η_2 when the TOP [Fig. 2(a)] is utilized in conjunction with the modified bridge distortion generator [Fig. 5(b)] and the conventional one [Fig. 2(c)]. For both cases, the parameters shown in Table II were utilized in the simulation. The resistor R for the example shown in Fig. 10 was calculated using (14) assuming that $\eta_2 = 1.2$ and $\eta_1 = 1$. Its value is 51 Ω. From the figure, it can be seen that the MRIM2 for the conventional configuration occurs at $\eta_2 = 1.2$. Its value is -48.4 dB. The MRIM2 for the modified configuration occurs at $\eta_2 = 1.1$ and its value is -84.9 dB. Consequently, the modified configuration has an MRIM2 36.5 dB lower than the one of the conventional one. It also should be noted that the IM3 generated by the conventional and modified bridge configurations are -32 and -38 dBm, respectively.

[4]It should be noted from (14) that when $g_{11} = g_{12}$ (that corresponds to the case when all diodes are identical), the resistor R is undetermined since the bridge is balanced and consequently the value of the resistor R does not affect the behavior of the circuit. The same occurs in (12) when $g_{11} = g_{13}$.

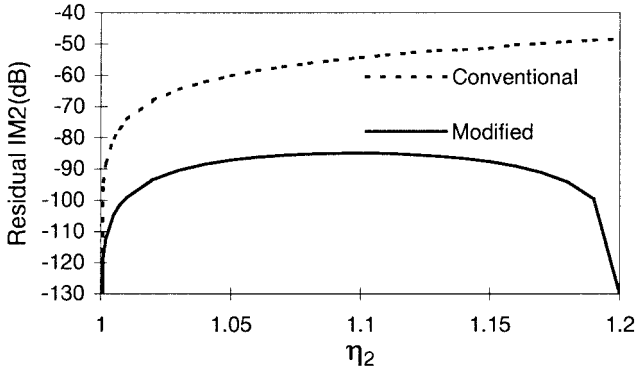

Fig. 10. Residual IM2 as a function of η_2 for the modified and conventional bridge configurations. It is assumed that $\eta_1 = \eta_4 = 1$ and $\eta_2 = \eta_3$. The resistor R was calculated assuming $\eta_2 = 1.2$.

The penalty for utilizing the resistor R is a 6-dB reduction in IM3.

Equation (14) can be rewritten as follows (see Appendix B)[5]:

$$R = -R_S + \frac{1}{g_{11}^{1/3}g_{12}^{2/3}} + \frac{1}{g_{12}^{1/3}g_{11}^{2/3}}. \tag{15}$$

It is important to mention that the value of R depends on the bias currents of the diodes since g_{11} and g_{12} depend on the bias current of the diodes D_1 and D_2, respectively. Equation (15) can be rewritten as follows:

$$R = r_1^{1/3}r_2^{2/3} + r_1^{2/3}r_2^{1/3} - R_S \tag{16}$$

where $r_1 = 1/g_{11}$ and $r_2 = 1/g_{12}$. Since $r_1 \approx r_2$, it can be concluded that

$$R \approx 2r_1 - R_S. \tag{17}$$

The total small signal resistance of two forward-biased diodes (D_A and D_B) in series is given by

$$R^* = R_{SA} + r_A + R_{SB} + r_B \tag{18}$$

where R_{SA} and R_{SB} and r_A and r_B are, respectively, the series resistances and the small signal junction resistances of diodes D_A and D_B. Assuming that $R_{SA} \approx R_{SB} \approx R_S$ and $r_A \approx r_B \approx r_1$,[6] R^* can be approximated by

$$R^* \approx 2(R_S + r_1). \tag{19}$$

Substituting R^*, given by (19), into (17) results in

$$R \approx R^* - 3R_S. \tag{20}$$

Equation (20) indicates that for $R^* \gg 3R_S$, the resistance R can be implemented by two diodes in series whose bias current is identical to the current that flows through the diodes that constitute the bridge. With this approach, the modified bridge configuration can work over a range of bias currents.

[5]It should be noted that (14) and (15) are equivalent, except for the case when $g_{11} = g_{12}$.

[6]It is implicitly understood that the bias current that flows through diodes D_A and D_B is almost identical to the currents that flow through the diodes of the bridge.

TABLE II
DIODES' PARAMETERS, RESISTOR VALUES, CURRENTS, AND VOLTAGES USED IN THE SIMULATION OF THE MODIFIED AND CONVENTIONAL BRIDGE CONFIGURATIONS

η_{min}	η_{max}	$\eta_1=\eta_4$	$\eta_2=\eta_3$	$R_{S1}=R_{S4}$	$R_{S2}=R_{S3}$	T
1	1.2	1	1-1.2	5 Ω	5 Ω	300 K
$I_{B1}=I_{B4}$	$I_{B2}=I_{B3}$	$R_1=R_2$	R_3	R_g	R_L	$P_g=V_g^2/R_g$
1 mA	1 mA	10 Ω	80 Ω	75 Ω	75 Ω	0 dBm

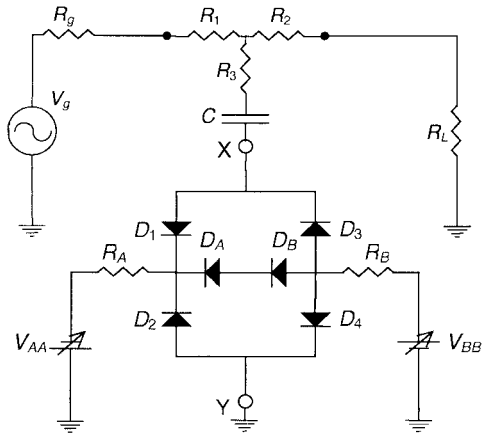

Fig. 11. Third-order predistorter implemented with a modified bridge configuration in which R is implemented by two diodes in series. The dc bias currents of the diodes can be changed by adjusting the dc voltage sources V_{AA} and V_{BB}.

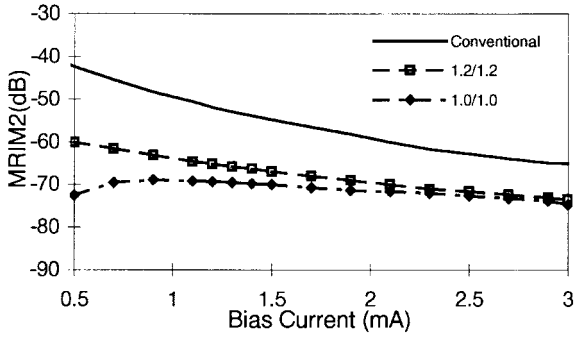

Fig. 12. MRIM2 of the bridge configuration as a function of the bias current of the diodes for the case where the resistor R is implemented by two Schottky diodes.

Fig. 11 shows a TOP using the modified bridge configuration when the resistor R is implemented by two diodes in series. As can be observed, diodes D_A and D_B are biased using the same bias circuit utilized by the other diodes. It should be noted that the third-order generator shown in Fig. 11 can be easily implemented in an IC.

Fig. 12 shows the MRIM2 of the circuit shown in Fig. 11 as a function of the diode's bias current.[7] Simulation results are presented for different ideality factors of the diodes that implement R. For comparison purposes, the MRIM2 as a function of the diodes' bias current for the TOP with a conventional bridge configuration is also shown in the figure. Simulation results shown in Fig. 12 assumed that diodes D_1 and D_4, as well as diodes D_2 and D_3, are, respectively, identical. The parameters shown in Table II were used for the simulation. The bridge diodes have $\eta_1 = \eta_4 = 1$ and $\eta_2 = \eta_3 = 1.2$. It can be observed that for low bias currents, the MRIM2 of the modified bridge configuration is about 18 dB better than that of the conventional one. At higher currents, the improvement is reduced to about 10 dB. This is due to the fact that the values of the small signal junction resistance of the diodes at high bias currents are of the same order of magnitude as the series resistance of the diodes. This can be clearly seen from Fig. 13, where the resistor R, calculated using (15), and R^* are shown as a function of the diode's bias current. For comparison purposes, the simulation of the resistance of the diodes was done for two diode pairs: the first pair has ideality factors $\eta_A = \eta_B = 1$ and the second pair $\eta_A = \eta_B = 1.2$. The difference between R and R^* is larger when $\eta_A = \eta_B = 1.2$.

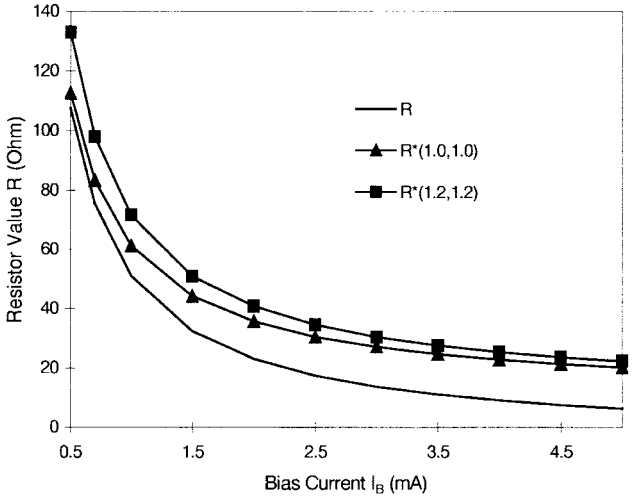

Fig. 13. R^* and R as a function of I_B. R^* is calculated for $\eta_A = \eta_B = 1\,[R^*(1.0,\ 1.0)]$ and $\eta_A = \eta_B = 1.2\,[R^*(1.2,\ 1.2)]$.

The application of the six-diode configuration is limited to relatively low bias currents. However, in many applications, the bias currents are normally low since high IM3 are required. For these applications, the possibility of implementing the resistor R using two diodes in series is very attractive.[8]

[7] It can be proven that the bias currents that flow for each diode are approximately equal, even though their ideality factors are different. This is due to the fact that, in general, the values of the external bias resistor R_A and R_B are large enough to set the bias currents through the diodes. Therefore, for the analysis, it is assumed that all the currents are identical.

[8] Since R^* is always larger than the optimum R, a resistor R_p could be placed in parallel with R^*. The value of R_p could be optimized to minimize the error between the overall resistance and R over a larger range of bias

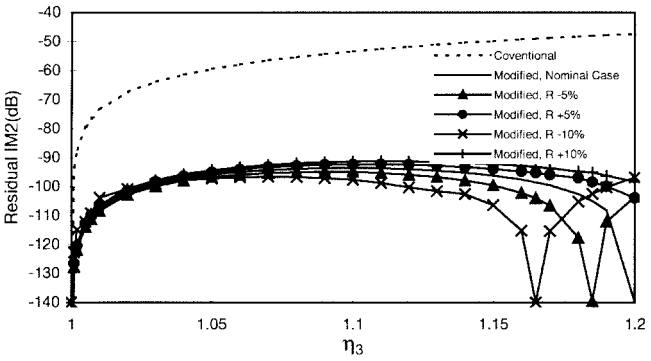

Fig. 14. Residual IM2 degradation in the modified antiparallel configuration due to the tolerances of the resistor R. The nominal value of R is 680 Ω. Tolerances are set to ±5 and ±10%.

The overall performance of the six-diode configuration can be substantially improved by choosing diodes with smaller series resistance. It is interesting to note that diodes D_A and D_B may generate certain distortion since they are nonlinear elements. However, their contribution to the overall residual IM2 or to the generation of IM3 is expected to be negligible since the ac voltage across them is small.

IV. Sensitivity Analysis

The objective of this section is to see how the component tolerances and the variations in temperature and in bias conditions affect the residual IM2 of the modified antiparallel and bridge configuration. The analysis will help to identify those components that are critical in the design of the circuits.

A. Sensitivity Analysis for the Modified Antiparallel Configuration

The nominal values utilized for the analysis of the modified antiparallel configuration are $R = 680\,\Omega$, $R_d = 60\,\Omega$, $I_B = 1$ mA, and $T = 300$ K. The nominal MRIM2 is -93.5 dB. The behavior of the circuit under the nominal conditions was presented in Fig. 8.

1) Resistor Tolerances: Fig. 14 shows the simulated residual IM2 as a function of η_3 assuming that the tolerances of the resistor R are set to ± 5 and $\pm 10\%$. It can be observed that the highest MRIM2 occurs when R is 10% larger than its nominal value. The penalty is an MRIM2 1 dB higher than the one for the nominal case. It can be seen that relatively large changes in R do not significantly degrade the residual IM2.

It is interesting to consider the case where the two resistors R_d that constitute the modified antiparallel configuration are different from each other. Fig. 15 shows the modified antiparallel configuration, where the resistors R_d are substituted by the resistors R_{d2} and R_{d4}. Fig. 16 shows the simulated residual IM2 as a function of η_3 when the difference between R_{d2} and R_{d4} is $\pm 1\%$ of the nominal value of R_d. It can be observed that the MRIM2 occurs when $R_{d2} - R_{d4} = +0.01\,R_d$ and its value is 17.7 dB higher than the one corresponding to the nominal case. This large change in MRIM2 makes R_d a critical component in the design of this circuit.

currents. Consequently, the predistorter could operate with smaller MRIM2 over a larger range of bias current.

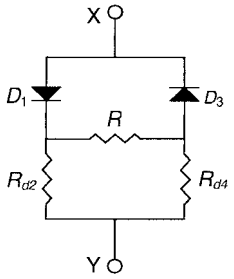

Fig. 15. Modified antiparallel configuration. For the nominal case $R_{d2} = R_{d4} = R_d$. Due to the tolerance of the components, in general, $R_{d2} \neq R_{d4}$.

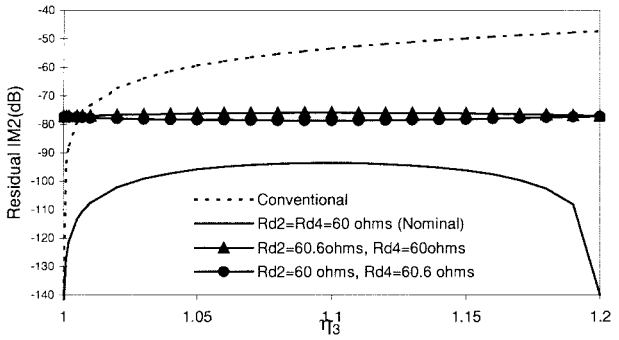

Fig. 16. Residual IM2 degradation in the modified antiparallel configuration due to mismatch in the values of R_d.

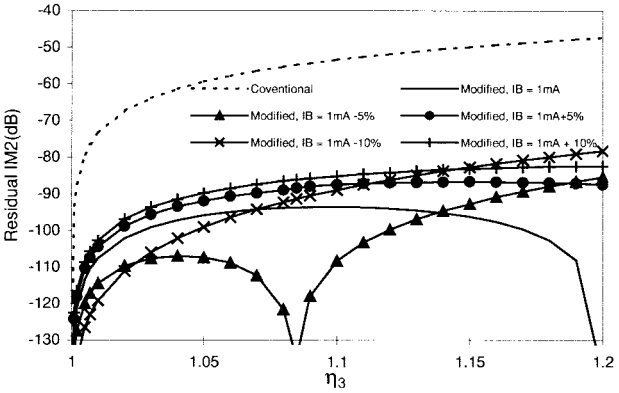

Fig. 17. Residual IM2 degradation in the modified antiparallel configuration due to changes in the bias current of the diodes.

2) Bias Current Tolerances: Fig. 17 shows the case when the diode currents change ± 5 and $\pm 10\%$ from their nominal value. From the figure, it can be observed that the MRIM2 is 15.3 higher than the nominal one. This value corresponds to $I_B = 0.90$ mA ($I_B - 10\%$). This indicates that changes in bias currents have to be limited to achieve good MRIM2.

3) Temperature Variations: Fig. 18 shows the simulated residual IM2 as a function of η_3 for three different temperatures (260, 300, and 340 K). Note that 300K is the nominal value. It can be observed that MRIM2 is 16 dB higher than the nominal value.

In summary, the two major contributors to the degradation of the MRIM2 are the resistors R_d and temperature.

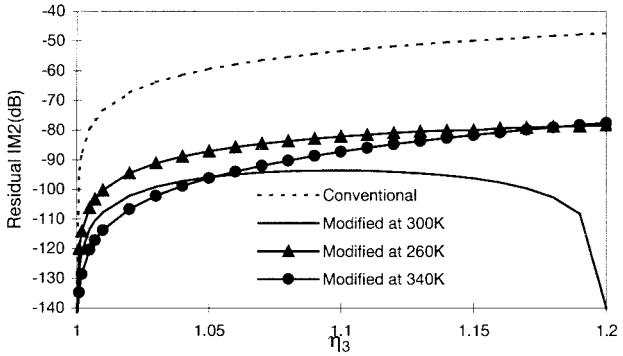

Fig. 18. Residual IM2 degradation in the modified antiparallel configuration due to small changes in temperature.

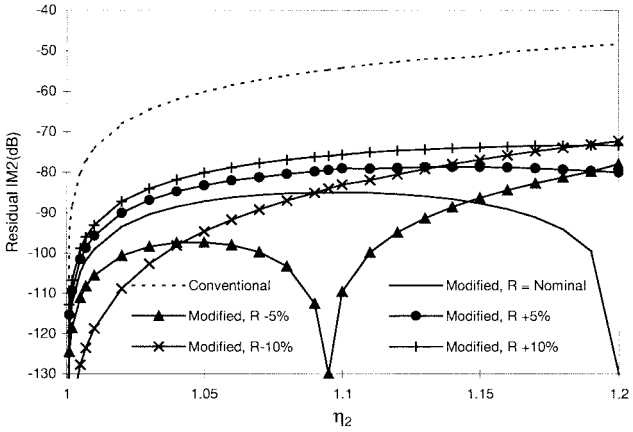

Fig. 19. Residual IM2 degradation in the modified bridge configuration due to tolerances in the resistor R. The nominal value of R is 51 Ω.

B. Sensitivity Analysis for the Modified Bridge Configuration

The nominal values utilized for the analysis of the modified bridge configuration are: $R = 51\ \Omega$, $I_B = 1$ mA, and $T = 300$ K. The nominal MRIM2 is -84.9 dB. The behavior of the circuit under the nominal conditions was presented in Fig. 10.

1) Resistor Tolerances: Fig. 19 shows the simulated residual IM2 as a function of η_2 assuming that the tolerances of the resistor R are set to ±5 and ±10% of its nominal value. From the figure, it can be observed that the highest MRIM2 occurs when the resistor is 10% smaller than its nominal value. The penalty is an MRIM2 12.7 dB higher than the nominal one. However, this penalty can be reduced to around 1 dB if the resistor is kept within ±1% tolerance. The nominal value of R is 51 Ω.

2) Bias Currents: Fig. 20 shows the case when the current that flows through the diodes changes ±5% from the nominal value. The MRIM2 occurs when the diode current is 5% higher than its nominal value. It should be noted that the penalty in the MRIM2 of the circuit, in comparison to the nominal case, is 6.8 dB. This effect could be reduced by limiting the bias current variation.

3) Temperature Variations: Fig. 21 shows the simulated residual IM2 as a function of η_2 for three different temperatures (260, 300, and 340K). The MRIM2 over the range of temperature is 15.5 dB higher than the nominal one. In summary, temperature is the main parameter that limits the performance of the modified bridge configuration. However, the MRIM2 over the range of temperatures is 21 dB lower than the MRIM2 of the conventional configuration.

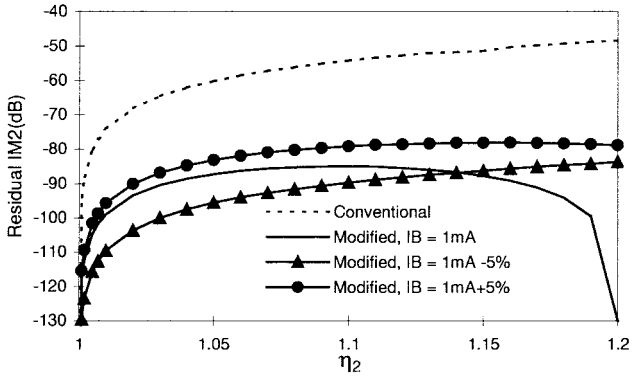

Fig. 20. Residual IM2 degradation in the modified bridge configuration due to small changes in the diode bias currents.

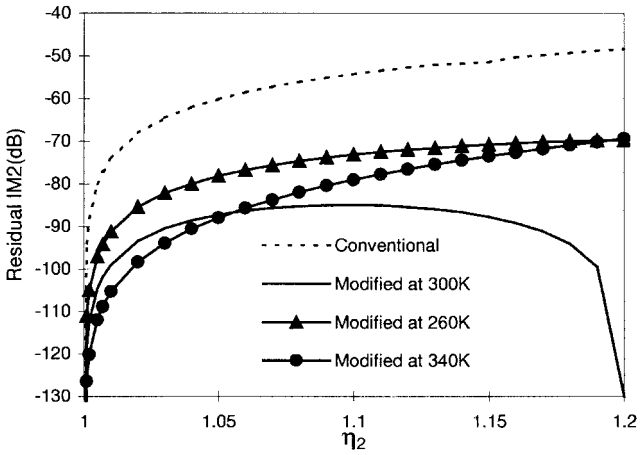

Fig. 21. Residual IM2 degradation in the modified bridge configuration due to changes in temperature.

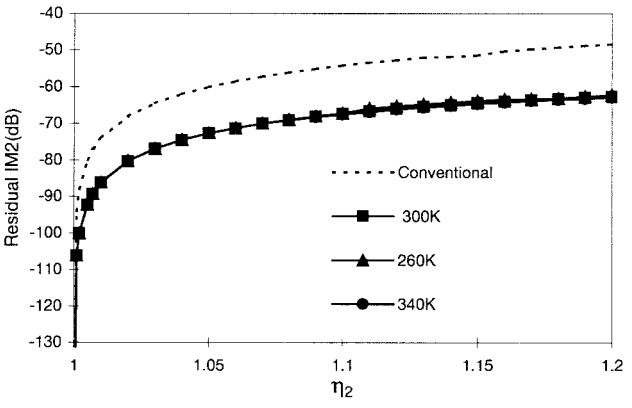

Fig. 22. Residual IM2 for the six-diode configuration as a function of η_2 for different temperatures.

C. Effect of Temperature on the Six-Diode Configuration

To simulate the effect of temperature in the six-diode configuration, it is assumed that the nominal conditions are $I_B = 1$ mA, $T = 300$K. The parameters given in Table II were used in the simulation. Fig. 22 shows the residual IM2 as a function of

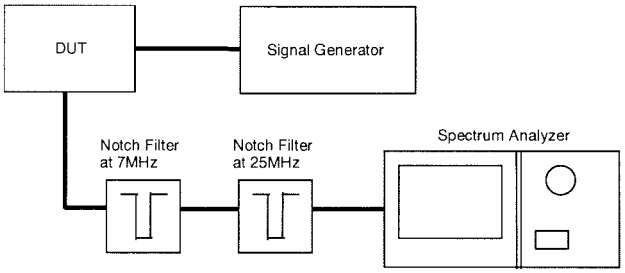

Fig. 23. Experimental setup utilized to measure the residual IM2 of the circuits.

η_2 for three different temperatures (260, 300, and 340K). It can be observed that the MRIM2 remains constant over temperature. This is due to the fact that the resistor R is implemented with two diodes in series whose resistances are also functions of the temperature. This is another advantage of the six-diode configuration. For the simulation $\eta_A = \eta_B = 1.2$.

V. Experimental Results

Two TOP's were implemented: one using the conventional antiparallel configuration and the other using the modified version. For both cases, the same pair of HP HSMS2820 Schottky diodes was utilized to implement the circuits. The measured characteristics of the diodes were those shown in Table I. D_3 has an ideality factor $\eta_3 = 1.2$. The measurements were performed using the setup shown in Fig. 23. The measured residual IM2 of the modified configuration was 20 dB lower than the measured residual IM2 of the conventional one. For the modified configuration, $R_d = 47\ \Omega$, $R = 180\ \Omega$, and I_B was set to 1.5 mA. For the measurements, the fundamental frequencies were set to $f_1 = 7$ MHz and $f_2 = 25$ MHz. IM2 was measured at 18 and 32 MHz. Notch filters were utilized in the measurement setup to improve the dynamic range of the network analyzer.

VI. Conclusion

In this paper, a novel technique was presented that reduces the generation of residual IM2 in third-order predistorters using antiparallel and bridge configurations. A detailed analysis of the circuits was carried out using the method of nonlinear currents. The analysis proved that, in theory, complete cancellation of the residual IM2 is achieved not only when the diodes are identical but also when the diodes are dissimilar. Since the dissimilarity of the diodes is due in great part to the random nature of the values of their ideality factors, the concept of MRIM2 was introduced to have an absolute measurement of the performance of the circuit when the ideality factors of the diodes are in the interval $[\eta_{\min}\ \eta_{\max}]$. Simulations carried out using CNL/2 proved that the MRIM2 of the new circuits was much lower than the ones of the conventional antiparallel and bridge configurations. A sensitivity analysis showed that two of the components (R_{d2} and R_{d4}) in the modified antiparallel configuration must have very small tolerances in order to reduce the degradation in their MRIM2. However, the MRIM2 of the modified bridge configuration proved to be quite insensitive to some of the changes that were tested, such as component tolerance and diode bias current variations. Its performance is limited by the temperature of operation of the circuits. It is important to mention that for a (diode) junction temperature range between 260–340 K, the simulated MRIM2 was 21 dB lower than the one corresponding to the equivalent conventional configuration.

A limitation of the modified bridge configuration shown in Fig. 5(b) is that it cannot operate over a range of bias currents without having a significant degradation in the MRIM2 of the circuit. A novel circuit, in which R is implemented by two diodes in series, was proposed and analyzed. The analysis showed that the new configuration has a good MRIM2 at low bias currents. Moreover, the MRIM2 of the configuration is quite insensitive to temperature variations.

For comparison purposes, a modified antiparallel configuration and a conventional one were implemented utilizing the same diodes. Experimental results showed that the MRIM2 of the modified configuration was 20 dB lower than the one obtained for the conventional configurations.

It should be noted that even though the calculation of R is carried out at $\eta_3 < 1.2$, it is still assumed that the statistical distribution of η_3 is between 1 and 1.2.

It should be noted from (14) that when $g_{11} = g_{12}$ (that corresponds to the case when all diodes are identical), the resistor R is undetermined since the bridge is balanced, and consequently, the value of the resistor R does not affect the behavior of the circuit. The same occurs in (12) when $g_{11} = g_{13}$.

It should be noted that (14) and (15) are equivalent, except for the case when $g_{11} = g_{12}$.

It is implicitly understood that the bias current that flows through diodes D_A and D_B is almost identical to the currents that flow through the diodes of the bridge.

It can be proven that the bias currents that flow for each diode are approximately equal, even though their ideality factors are different. This is due to the fact that, in general, the values of the external bias resistor R_A and R_B are large enough to set the bias currents through the diodes. Therefore, for the analysis, it is assumed that all the currents are identical.

Since R^* is always larger than the optimum R, a resistor R_p could be placed in parallel with R^*. The value of R_p could be optimized to minimize the error between the overall resistance and R over a larger range of bias currents. Consequently, the predistorter could operate with smaller MRIM2 over a larger range of bias current.

Appendix A

Rearranging the denominator of (12), as shown in (A1.1), results in (A1.2), both shown at the top of the following page. Dividing numerator and denominator by $g_{11}^{2/3}(g_{13}R_s + 1) - g_{13}^{2/3}(g_{11}R_s + 1)$ results in

$$R = \frac{2}{-\dfrac{1}{R_d} + \dfrac{g_{13}^{2/3}g_{11} - g_{11}^{2/3}g_{13}}{g_{11}^{2/3}(g_{13}R_s + 1) - g_{13}^{2/3}(g_{11}R_s + 1)}}. \quad \text{(A1.3)}$$

$$R=\frac{2\left[g_{11}^{2/3}(g_{13}R_s+1)-g_{13}^{2/3}(g_{11}R_s+1)\right]}{g_{13}^{2/3}\left[\frac{1}{R_d}(g_{11}R_s+1)+g_{11}\right]-g_{11}^{2/3}\left[\frac{1}{R_d}(g_{13}R_s+1)+g_{13}\right]} \tag{A1.1}$$

$$R=\frac{2\left[g_{11}^{2/3}(g_{13}R_s+1)-g_{13}^{2/3}(g_{11}R_s+1)\right]}{\frac{1}{R_d}\left[g_{13}^{2/3}(g_{11}R_S+1)-g_{11}^{2/3}(g_{13}R_s+1)\right]+g_{13}^{2/3}g_{11}-g_{11}^{2/3}g_{13}} \tag{A1.2}$$

Rearranging the second term of the denominator results in

$$R=\frac{2}{-\frac{1}{R_d}+\frac{g_{13}^{2/3}g_{11}-g_{11}^{2/3}g_{13}}{R_s(g_{11}^{2/3}g_{13}-g_{13}^{2/3}g_{11})+g_{11}^{2/3}-g_{13}^{2/3}}}. \tag{A1.4}$$

Dividing the numerator and denominator of the second term of the denominator by $g_{13}^{2/3}g_{11}-g_{11}^{2/3}g_{13}$ results in

$$R=\frac{2}{-\frac{1}{R_d}+\frac{1}{-R_s+\frac{g_{11}^{2/3}-g_{13}^{2/3}}{g_{13}^{2/3}g_{11}-g_{11}^{2/3}g_{13}}}}. \tag{A1.5}$$

Rearranging the second term of the denominator results in

$$R=\frac{2}{-\frac{1}{R_d}+\frac{1}{-R_s+\frac{\left(g_{11}^{1/3}-g_{13}^{1/3}\right)\left(g_{11}^{1/3}+g_{13}^{1/3}\right)}{g_{11}^{2/3}g_{13}^{2/3}\left(g_{11}^{1/3}-g_{13}^{1/3}\right)}}}. \tag{A1.6}$$

For $g_{11}\neq g_{13}$, (A1.6) can be simplified to

$$R=\frac{2}{-\frac{1}{R_d}+\frac{1}{-R_s+\frac{g_{11}^{1/3}+g_{13}^{1/3}}{g_{11}^{2/3}g_{13}^{2/3}}}}. \tag{A1.7}$$

Since $R\geq 0$, the denominator of (A1.7) must be larger or equal to zero

$$-\frac{1}{R_d}+\frac{1}{-R_s+\frac{g_{11}^{1/3}+g_{13}^{1/3}}{g_{11}^{2/3}g_{13}^{2/3}}}\geq 0 \tag{A1.8}$$

or equivalently,

$$R_d\geq\frac{g_{11}^{1/3}+g_{13}^{1/3}}{g_{11}^{2/3}g_{13}^{2/3}}-R_S=R_{d\,\min}. \tag{A1.9}$$

From (A1.7), it can be clearly seen that when $R_d=R_{d\,\min}$, $R\rightarrow\infty$.

APPENDIX B

From (14)

$$R=\frac{g_{11}^{2/3}(g_{12}R_s+1)-g_{12}^{2/3}(g_{11}R_s+1)}{g_{11}g_{12}^{2/3}-g_{12}g_{11}^{2/3}}. \tag{A2.1}$$

Rearranging the numerator results in

$$R=\frac{R_S(g_{11}^{2/3}g_{12}-g_{12}^{2/3}g_{11})+g_{11}^{2/3}-g_{12}^{2/3}}{g_{11}g_{12}^{2/3}-g_{12}g_{11}^{2/3}}. \tag{A2.2}$$

This equation can be rewritten as

$$\begin{aligned}R&=-R_S+\frac{g_{11}^{2/3}-g_{12}^{2/3}}{g_{11}g_{12}^{2/3}-g_{12}g_{11}^{2/3}}\\&=-R_S+\frac{\left(g_{11}^{1/3}-g_{12}^{1/3}\right)\left(g_{11}^{1/3}+g_{12}^{1/3}\right)}{g_{11}^{2/3}g_{12}^{2/3}\left(g_{11}^{1/3}-g_{12}^{1/3}\right)}.\end{aligned} \tag{A2.3}$$

Finally, for $g_{11}\neq g_{12}$,

$$R=-R_S+\frac{1}{g_{11}^{1/3}g_{12}^{2/3}}+\frac{1}{g_{12}^{1/3}g_{11}^{2/3}}. \tag{A2.4}$$

ACKNOWLEDGMENT

The authors would like to thank Dr. H. Chou of Harmonic Lightwaves, Inc., for supporting and encouraging this work and G. Ries of Alcatel Network System, Inc., for his careful review of the manuscript.

REFERENCES

[1] M. Nazarathy *et al.*, "Predistorter for high frequency optical communication devices," U.S. patent 5 424 680, 1995.
[2] H. Blauvelt *et al.*, "Predistorter for linearization of electronic and optical signals," U.S. patent 4 992 754, 1991.
[3] L. Zhang *et al.*, "Ten-GHz MMIC predistortion circuit for improved dynamic range of broadband analog fiber-optic link," *Microwave Opt. Technol. Lett.*, vol. 11, no. 6, pp. 293–295, 1996.
[4] M. Di Benedetto *et al.*, "A new analog predistortion criterion with application to high efficiency digital radio systems," *IEEE Trans. Commun.*, vol. 43, pp. 2966–2974, 1995.
[5] J. Grebliumas *et al.*, "Microwave predistortion linearizer," U.S. patent 5 523 716, 1996.
[6] R. Hecken, "Signal cuber circuits," U.S. patent 4 157 508, 1979.
[7] S. Maas, *CNL/2, Non-Linear Simulation Program.* Norwood, MA: Artech, 1996.
[8] S. Maas, *Non-Linear Microwave Circuits.* Norwood, MA: Artech, 1988.
[9] A. Rrochazka *et al.*, "High frequency distortion analysis of a semiconductor diode for CATV applications," *IEEE Trans. Consumer Electron.*, vol. CE-21, no. 2, pp. 120–124, 1975.

Wei Huang (S'85–M'86) received the B.S.E.E. and M.S.E.E. degrees from the State University of New York at Stony Brook in 1985 and 1986, respectively. His field of concentration was in digital signal processing.

From 1986 to 1990, he was a Design Engineer at Viewsonics, Syosset, NY, where he designed various RF communication devices and equipment. In 1990, he joined Philips Broadband Networks, Manlius, NY, as a Design Engineer. He was the Project Team Leader for CATV network amplifiers and optical node stations for hybrid fiber coax (HFC) networks. He was involved in the design and development of optical receivers and transmitters. He was promoted to Staff Engineer and was involved in the analysis of broad-band RF predistortion circuitry. Since 1995, he has been a Member of Technical Staff at Harmonic Lightwaves, Sunnyvale, CA, where he has been involved in the design and development of optical node stations, predistortion circuits for RF amplifiers and directly modulated laser transmitters, return path optical receivers and transmitters, and linearization for external modulators. He is currently the Manager of the Receivers and Return Path Product Group.

Mr. Huang is a member of Tau Beta Pi and Eta Kappa Nu.

Ricardo E. Saad (S'94–M'96) received the electrical engineering diploma with first class honors from Cordoba National University, Argentina, in 1986, the M.Sc. degree with distinction award in electrical engineering from the State University of Campinas, Brazil, in 1989, and the Ph.D. degree in electrical engineering from the University of Toronto, Canada, in 1996.

He is presently working for Alcatel Network Systems, TX, where he is involved in the research and development of high-speed optical systems for DWDM optical networks. He previously worked for Harmonic Lightwaves, Sunnyvale, CA, where he was the Project Leader for the research and development of directly modulated optical transmitters for CATV. From 1987 to 1990, he was with the Research and Development Center of the Brazilian Telecommunication Holding Company (CPqD-Telebras) where he conducted research in high-speed receivers for optical communications. From 1991 to 1996, he was with the Computer Integrated Manufacturing Laboratory, University of Toronto, where he carried out research in optical sensing. His interests currently include optical communications, high-speed optoelectronics, microwaves, and optical sensing. He coauthored two sections in the book entitled *The Measurement, Instrumentation, and Sensor Handbook*, (Boca Raton, FL: CRC Press, 1998), and 18 papers in refereed journals and international conferences.